

# **Characterization of 70k Toba Ash from Dahigaon, upland Deccan Traps, India**

A Thesis

submitted to

Indian Institute of Science Education and Research Pune in partial fulfillment of the  
requirements for the BS-MS Dual Degree Programme

by

Parag Hembram



Indian Institute of Science Education and Research Pune  
Dr. Homi Bhabha Road,  
Pashan, Pune 411008, INDIA.

April, 2024

Supervisor: Dr. Raymond A. Duraiswami

Parag Hembram 2024

All rights reserved

## Certificate

This is to certify that this dissertation entitled “Characterisation of 70k Toba Ash from Dahigaon, upland deccan trap sites” towards the partial fulfillment of the BS-MS dual degree programme at the Indian Institute of Science Education and Research, Pune represents study/work carried out by Parag Hembram at Indian Institute of Science Education and Research and Savitribai Phule Pune University under the supervision of Dr. Raymond A. Duraiswami, Professor, Department of Geology, during the academic year 2023-2024.

A handwritten signature in black ink, appearing to read 'R. DURAISWAMI', is written diagonally across the page.

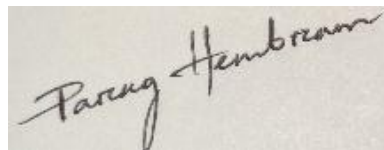
Dr. Raymond A. Duraiswami

Committee:

Dr. Raymond A. Duraiswami

# Declaration

I hereby declare that the matter embodied in the report entitled “Characterization of 70k Toba Ash from Dahigaon, upland Deccan Trap sites” Here are the results of the work carried out by me at the Department of Geology, Indian Institute of Science Education and Research, Pune and Savitribai Phule Pune University under the supervision of Dr. Raymond A. Duraiswami and the same has not been submitted elsewhere for any other degree.

A photograph of a handwritten signature in black ink on a light-colored background. The signature is written in a cursive style and reads "Parag Hembram".

Parag Hembram

Date: 27.03.2024

# Table of Contents

<b>Abstract.....</b>	<b>7</b>
<b>Acknowledgments.....</b>	<b>8</b>
<b>1. Introduction.....</b>	<b>10</b>
1.1 Geology.....	13
<b>2. Materials and Methods.....</b>	<b>16</b>
2.1. Petrography.....	16
2.1.1 Principle.....	16
2.2. X-ray fluorescence.....	17
2.2.1. Principle.....	17
2.2.2. Why Did we do XRF?.....	17
2.2.3. Fusion Bead preparation.....	17
2.3. X-ray diffraction.....	19
2.3.1. Principle.....	19
2.3.2. Bragg's law.....	19
2.4. SEM.....	21
2.4.1. Principle.....	21
2.4.2. Why did we do SEM?.....	21
2.5. ICPMS.....	22
2.5.1. Principle.....	22
2.5.2. Sample Preparation.....	22
<b>3. Results and discussions.....</b>	<b>25</b>
<b>4. Conclusion.....</b>	<b>40</b>
<b>5. Bibliography.....</b>	<b>43</b>

## List of figures

Fig. 1.1: Google image of the area.....	11
Fig. 1.2: Field photographs of Quaternary sediments exposed in the study area.....	12
Fig. 1.3: Field photographs of the ash horizon exposed n the Quaternary sediments in the study area.....	13
Fig 2.1: (a) & (b) Petrographic microscope.....	16
Fig 2.2: (a) Fusion Bead machine (b) Fusion beads (c) XRF analyzer.....	19
Fig 2.3: X-ray diffractometer.....	20
Fig 2.4: SEM .....	21
Fig 2.5: Sample digestion on hot plate .....	23
Fig 3.1: Photographs showing morphology of volcanic glass from ash .....	26
Fig 3.2: Scanning Electron Microscopy (SEM) of ash from present study.....	27
Fig 3.3: Scanning Electron Microscopy (SEM) of pumecious shards from present study...28	
Fig 3.4: Scanning Electron Microscopy (SEM of pumecious shards from reworked network.....	29
Fig 3.5: XRD patterns of A2 and A5 sample .....	32
Fig 3.6: Graphs of Mg number vs various oxides .....	35
Fig 3.7: Graphs of SiO <sub>2</sub> versus various oxides.....	36
Fig 3.8: TAS diagram .....	36
Fig 3.9: Plot of Primitive mantle versus elements.....	39

## List of tables

Table 3.1: Chemical composition of YTT glass shards in Lake Malawi, compared with proximal samples from the Toba caldera in Sumatra, Indonesia , YTT ash from the Indian archaeological site of Jwalapuram and Satara, Maharashtra.....	31
Table 3.2: A2 and A5 sample diffraction data for minerals.....	33
Table 3.3: Oxide percentage of volcanic ash samples.....	34

# Abstract

The eruption of the Toba super volcano approximately 75,000 years ago on the Indonesian island of Sumatra left behind extensive ash deposits known as Toba ash, marking one of the largest volcanic events in recorded history. The eruption's impact extended far beyond Sumatra, with Toba ash deposits discovered across Southeast Asia and beyond, including regions as distant as the Bay of Bengal, the South China Sea, and the eastern Indian Ocean. This widespread distribution underscores the eruption's colossal scale and its profound consequences for the environment and human populations of the time.

Toba ash is not confined to specific geological formations but has been found in diverse settings worldwide, from sedimentary records in Italy, Japan, and the Philippines to marine sediment cores in various oceanic regions. The eruption, characterized by a highly explosive Plinian phase, ejected immense volumes of ash, tephra, and pumice, blanketing vast swathes of central Sumatra and adjacent areas in South Asia. The presence of Toba ash in sedimentary archives globally attests to its significant impact on the Earth's climate and ecosystems.

This research project focuses on the detailed study and characterization of Toba ash deposits located in Morgaon and Bori within the Pune District of Maharashtra, India, as well as a potential new site in the Satara District. The investigation employs advanced petrological and scanning electron microscopy (SEM) techniques to analyze the physical and mineralogical properties of the ash. Additionally, mineralogical analysis of associated minerals will be conducted using advanced methods such as Raman spectroscopy, X-ray diffraction (XRD), and geochemical analysis through X-ray fluorescence (XRF) and laser ablation inductively coupled plasma mass spectrometry (LA-ICP-MS). Through this interdisciplinary approach, the study aims to provide valuable insights into the characteristics and implications of Toba ash deposits in the Indian context and contribute to our understanding of past volcanic events and their global impacts.

# Acknowledgments

I am deeply grateful to my thesis Supervisor, Dr. Raymond A. Duraiswami, for his unwavering support and guidance throughout my research journey. His constructive feedback helped me correct my mistakes in experimental work, and his ideas provided valuable solutions when I was stuck.

I am thankful to my thesis expert, Dr. Gyana Ranjan Tripathy, for his support in giving access to the lab to run my experiments.

I would like to express my gratitude to my batchmates for their continuous support and for bearing my poor jokes. I would also like to thank my badminton teammates for all the excellent matches we have played.

I would like to mention my close friends Vara, Ratan, Pranav, Sanket, Gopi, and Ashish for constantly being there for me throughout my research journey.

Finally, I would like to thank my Maa, Bapa, and my little brother, as well as my cousins, for their unwavering support.



# **CHAPTER-1**

## INTRODUCTION

The eruption of Mount Toba, estimated to have occurred approximately 75,000 years ago, stands out as one of the most remarkable volcanic events in Earth's history. This eruption is renowned for its colossal scale, involving the release of an immense volume of magma, surpassing  $7 \times 10^{18}$  grams. As a result, it ranks among the largest volcanic eruptions ever documented. The eruption ejected a vast quantity of volcanic material, primarily composed of rhyolitic magma, which spread over an extensive area, covering approximately 20,000-30,000 square kilometers.

In addition to the eruption's magnitude, it also produced a massive ash cloud known as a coignimbrite ash cloud, which dispersed widely across the atmosphere. This ash cloud, estimated to weigh around  $2 \times 10^{15}$  grams, blanketed a significant portion of Earth's surface with a layer of ash approximately 10 centimeters thick. The extent of this ash fallout was considerable, covering approximately 1% of the Earth's surface.

Despite the eruption originating in Sumatra, Indonesia, its impact was far-reaching, affecting regions well beyond its immediate vicinity. The dispersal of volcanic ash from the Toba eruption reached as far as the Indian subcontinent, with notable ash deposits found in areas such as the Deccan Trap region. This widespread distribution of Toba ash deposits in India presents a unique opportunity for researchers to study the aftermath of this volcanic event and its implications for regional geology and environmental dynamics.

The research project focuses on investigating Toba ash deposits in specific locations within Maharashtra, India, notably in Morgaon and Bori, situated in the Pune District. Additionally, the project aims to explore the possibility of identifying new ash deposit sites in the Satara District. By conducting detailed examinations of these ash deposits, researchers intend to uncover their distinctive features and gain insights into various aspects, including the geological processes involved in ash dispersal, the composition of volcanic materials, and their long-term effects on local landscapes and ecosystems.

Understanding the characteristics and distribution of Toba ash deposits in India is essential for comprehending the broader implications of this monumental volcanic event. The research endeavor seeks to contribute to our understanding of past volcanic eruptions and their impacts on Earth's dynamic systems. By elucidating the geological footprint of the Toba eruption in Maharashtra and beyond, scientists aim to enhance our knowledge of volcanic activity, geological processes, and environmental change over geological timescales. Through comprehensive analysis and interpretation, this research endeavors to provide valuable insights into the complex interactions between volcanic activity, geological processes, and environmental dynamics, ultimately contributing to our understanding of Earth's geological history.



**Fig. 1.1:** Google image of the area around Dahigaon showing the meandering Wasana River and the intensely cultivated flood plain. The volcanic ash (red star) exposed on the river bank in thick alluvium of Quaternary age







**Fig. 1.2:** Field photographs of Quaternary sediments exposed in the study area. (a) Thick section of Quaternary alluvium exposed in the bank of Wasana R. (b) Consolidated granule sand at the base of the section. (c) Semi-consolidated coarse sand containing quartz pebbles.(d) bed of coarse sand alternating with brown coloured silty mud.(e) Coarse sand lenses in silty mud. Note the presence of pebbles in the coarse sand.



**Fig. 1.3:** Field photographs of the ash horizon exposed in the Quaternary sediments in the study area.

### 1.1 Geology

The area around Dahigaon (Fig 1.1) is drained by the Wasana River, which meanders in a floodplain covered by thick river alluvium and rich black cotton soil. Towards the upper reaches of the Wasana River, thick Quaternary alluvium is exposed along the banks. In approximately a 6-meter-thick section (Fig 1.2), the sediments are underlain by an erosional surface composed of red vesicular vesicle belonging to the Deccan Traps. The base of the section consists of massive granular sand showing cement (Fig 1.2(b)). In other locations, the granular sand shows crude development of parallel lamination (Fig 1.2(c)). The granular sand contains occasional large pebbles of agate and quartz. The sandy granule unit at the base is overlain by approximately 1.5 meters of brown silty mud (Fig 1.2(d)). The silty mud contains a few thick to thin beds of pebbly matrix-supported sand. At the top of this unit is a 30 cm thick volcanic ash layer (Fig 1.3). The ash

is unconsolidated, fine-grained (less than 2mm), and can be traced as a white horizon for about 10 meters in the section. Small lenses of reworked ash are also seen in the brown silty mud (Fig 1.3). The ash horizon is overlain by 0.9 meters of brown clay, and towards the upper part, about 1.2 meters of light brown silty sand containing lenses of pebble-bearing granular sand are observed (Fig 1.2(e)). The top of the section is marked by a 0.36-meter-thick layer of dark brown soil that supports luxuriant vegetation.

# **CHAPTER-2**

## 2. MATERIALS AND METHODS

### 2.1 Petrography

Petrography involves studying rocks in thin sections using a special microscope called a petrologic microscope. This microscope uses polarized light that vibrates in a specific direction to examine the rocks more closely.

#### 2.1.1 Principle

Petrography is like looking closely at slices of rocks under a special microscope. We study the different minerals and how they're arranged in the rock. By doing this, we can figure out what type of rock it is and how it formed. This helps us understand what happened in the past to shape the Earth's surface and what conditions were like when the rocks were made.

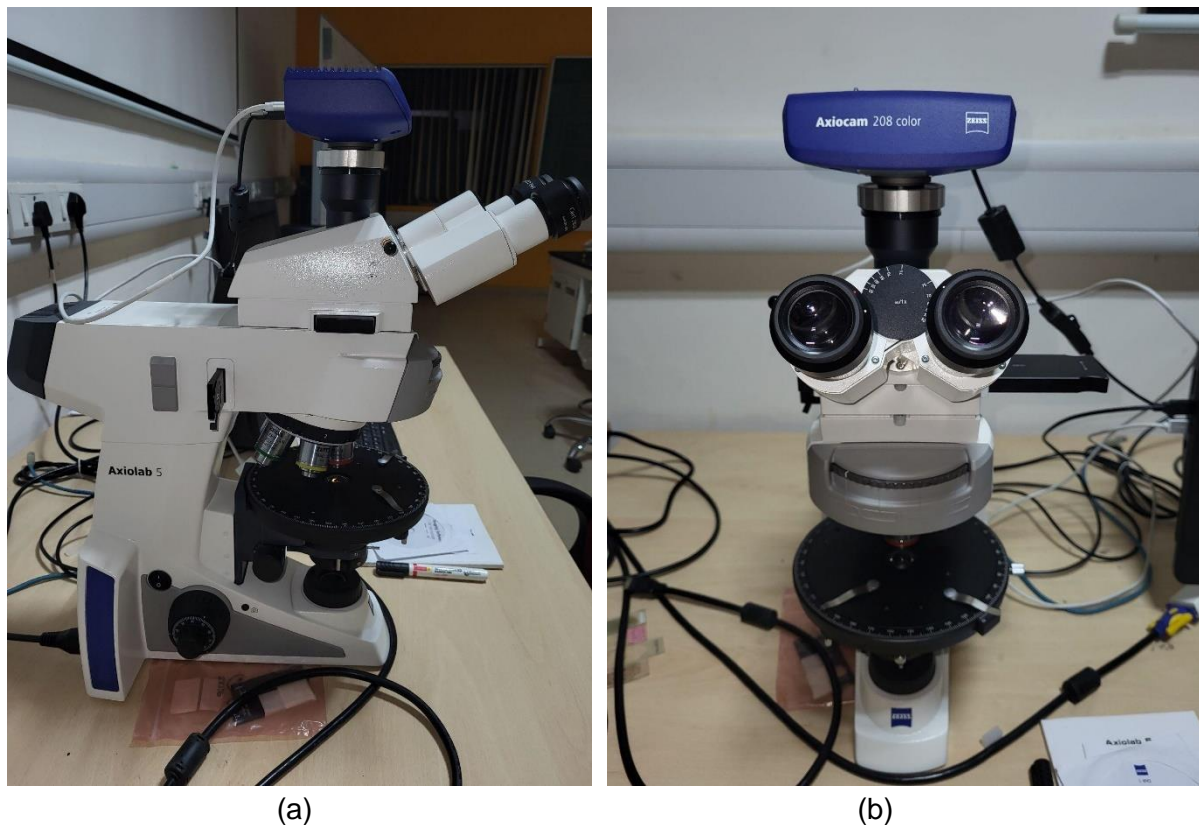


**Fig 2.1:** (a) & (b) Petrographic microscope

### 2.2 X-ray fluorescence

X-ray Fluorescence (XRF) is a technique used to analyze the elemental composition of materials without causing any damage to them. It operates by directing X-rays onto a sample, prompting the sample to emit its own X-rays. Each element emits distinct X-rays, akin to a fingerprint, enabling the identification of elements present in the sample. Consequently, XRF is highly effective for both qualitative and quantitative analysis of material composition.



### 2.2.1 Principle

X-ray Fluorescence (XRF) operates by exciting atoms within a sample. A primary X-ray, usually produced in an X-ray tube, interacts with an inner shell electron of an atom, causing it to be ejected. This vacancy is then filled by an electron from a higher energy shell, resulting in the emission of fluorescence radiation. The energy of this fluorescence radiation corresponds to the energy difference between the two electron shells, providing a unique characteristic for each atom and enabling the identification of the atoms present in the sample.

### 2.2.2 Why Did we do XRF?

Analyzing the Toba ash's elements helps create a unique chemical signature. This signature is like a fingerprint that we can compare to known volcanoes or references, helping us pinpoint where the ash came from and which volcano it originated from.

### 2.2.3. Powdering method

Before using the mortar and pestle, make sure they're clean and clear of any impurities that might harm your sample. Wash them well with the proper solvent and allow them to dry completely. Place the ash sample. Hold the pestle firmly with one hand and smash. Use downward pressure to break up the material into smaller particles. Monitor continually until the required particle size is achieved. Once the material has been thoroughly ground, transfer it to the chosen container. After usage, properly clean the agate mortar and pestle to eliminate any residual sample.

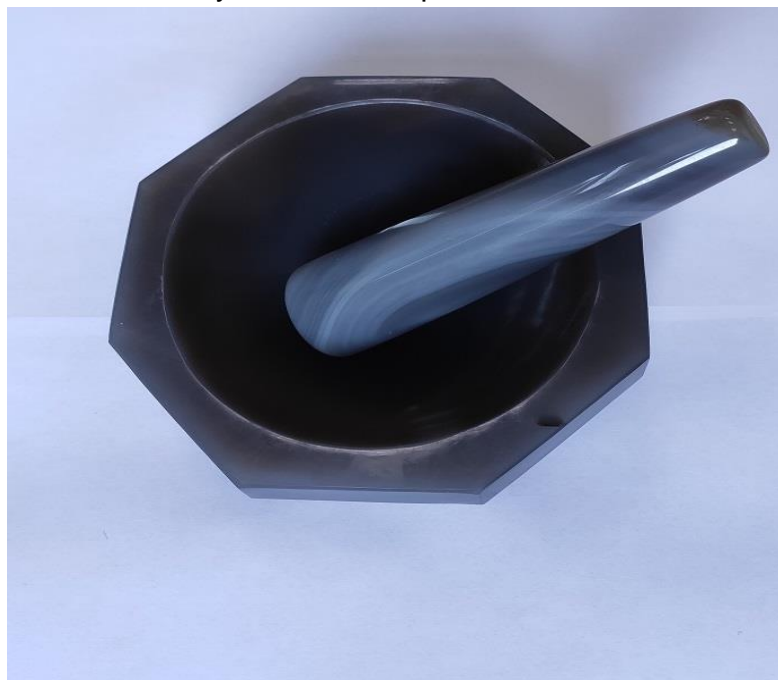


**Fig 2.2:** Agate mortar

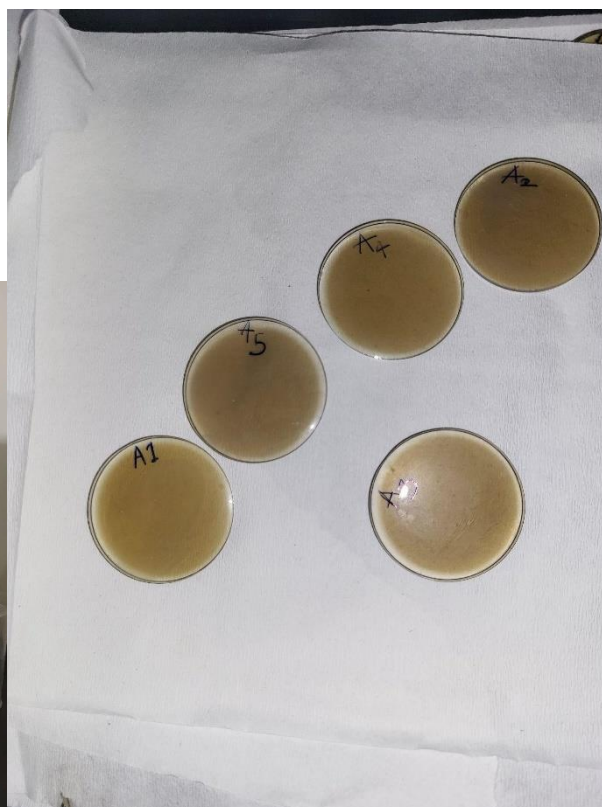
source: <https://www.canfortlab.com/Agate-Mortar-And-Pestle-p555.html>

#### 2.2.4. Fusion Bead preparation

- Take the crucible and place it on the weighing machine.
- Add 9.35 gm of flux and 0.55 gm of sample weight to the crucible.
- Add 10-12 drops of Releasing solution to the mixture in the crucible.
- Open the XRF machine by selecting “open door” and place the crucible and plate inside.
- Select “Acknowledge” on the XRF machine and then select “start” to begin the process.
- Allow the process to continue for 15 minutes.
- Wait for 15 minutes after the XRF buzzes.
- Use a vacuum to remove the bead from the crucible.
- After each bead preparation, clean the crucible using an ultrasonic cleaner.
- Place the crucible and plate in two beakers and add 2M-H<sub>2</sub>SO<sub>4</sub> to each beaker up to 150 ml.
- Put the beakers in the ultrasonic machine for 5 minutes.
- Clean the crucible and plate with XRF-MS.
- Clean the crucible and plate with propanol.
- The crucible is now ready for the next round of bead preparation.



(a)



(b)



(c)

**Fig 2.2:** (a) Fusion Bead machine (b) Fusion beads (c) XRF analyzer

## 2.3 X-ray diffraction

In geology, X-ray Diffraction (XRD) is a useful method for determining the mineral composition of rocks and soil. Geologists can identify minerals in a sample by exposing it to X-rays and analyzing the resultant diffraction patterns.

### 2.3.1 Principle

X-ray diffraction is like taking a special picture of a crystalline material, such as a mineral. It works by shooting X-rays at the material and measuring how they bounce off. When the X-rays hit the material at just the right angle, they bounce off in a specific direction, creating a pattern called diffraction. This pattern tells us about the arrangement of atoms in the material.

To get this pattern, we use a machine that generates X-rays and shoots them at the material. The X-rays are filtered to make them all the same wavelength and then focused onto the sample. When the X-rays hit the material, they bounce off in certain directions based on the arrangement of atoms in the crystal.

By scanning the sample through different angles, we can capture all the possible patterns of diffraction. Then, we compare these patterns to known patterns for different minerals to identify what the material is made of. Each mineral has a unique pattern, like a fingerprint, so we can match the patterns to figure out what mineral we're looking at.

### 2.3.2 Bragg's law

Bragg's law is a fundamental principle used in X-ray diffraction (XRD) analysis to determine the structure of crystalline materials, such as minerals in rocks. Bragg's law relates the angle of diffraction ( $\theta$ ), the wavelength of the X-rays ( $\lambda$ ), and the spacing between atomic planes in the crystal lattice ( $d$ ). It is expressed mathematically as:

$$n\lambda = 2d\sin\theta$$

$n$  is an integer representing the order of the diffraction peak

$\lambda$  is the wavelength of the X-rays

$d$  is the spacing between atomic planes in the crystal lattice

$\theta$  is the angle between the incident X-ray beam and the atomic planes

Bragg's law is a secret code that geologists use to determine which minerals are present in rocks using a method known as X-ray diffraction (XRD). When we beam X-rays at a rock, they bounce off the mineral crystals within. Bragg's rule allows us to unlock the code by measuring the angles at which these X-rays reflect off.

This code describes the distances between the layers of atoms within mineral crystals. Each mineral has a unique code, much like a fingerprint. So, by deciphering this code, we can determine which minerals are in the rock. This allows geologists to categorize rocks and comprehend what they're made of, which is critical for understanding the Earth's surface and history.



**Fig 2.3:** X-ray diffractometer at IISER, Pune

## 2.4 SEM

SEM (Scanning Electron Microscope) is a useful instrument for investigating the surface appearance, mineral content, and microstructure of geological materials. It enables geologists to analyze the tiny features of rocks, minerals, sediments, and other geological materials at extremely high magnification and resolution.

Geologists may use SEM to see mineral grains, crystal formations, textures, and surface roughness with extraordinary clarity. This knowledge aids in mineral identification, understanding rock formation and alteration processes, and interpreting geological phenomenon.

### 2.4.1. Principle

SEM (Scanning Electron Microscope) works by examining a sample's surface with a focused stream of electrons and producing high-resolution pictures. Unlike traditional optical microscopes, which use light waves to magnify and see materials, SEM uses electrons with significantly shorter wavelengths, allowing for increased magnification and resolution.

### 2.4.2. Why did we do SEM?

Studying SEM is important because they can provide valuable information about the eruption's source, eruption style, and the geological processes involved. Analyzing the composition and characteristics helps understand the history and impact of the Toba eruption.



**Fig 2.4:** SEM Lab at CIF, SPPU



## 2.5 ICP MS

ICP-MS (Inductively Coupled Plasma-Mass Spectrometry) is a method employed for the determination of low concentrations (typically in the parts per billion range, ppb, corresponding to  $\mu\text{g/l}$ ) as well as ultra-low concentrations of elements (typically in the parts per trillion range, ppt, equivalent to  $\text{ng/l}$ ). In this technique, atomic elements are introduced into a plasma source where they undergo ionization. Following ionization, these ions are separated based on their mass.

### 2.5.1. Principle

The sample undergoes atomization and ionization within the high-temperature plasma, producing ions that are subsequently extracted through the interface region and directed into a series of electrostatic lenses known as the ion optics. These ion optics serve to concentrate and direct the ion beam toward the quadrupole mass analyzer. Within the mass analyzer, ions are sorted based on their mass-to-charge ratio ( $m/z$ ), and the resulting ions are detected for measurement purposes.



**Fig 2.4:** ICP-MS (Inductively coupled plasma mass spectrometry) Lab at CIF, SPPU

### 2.5.2. Sample Preparation

- 0.100 grams of the sample was measured and transferred into a volumetric flask.
- 3ml of Aqua regia was prepared in a 1:3 ratio of  $\text{HNO}_3$  to  $\text{HCl}$ , which was used to digest the solid samples.
- This mixture of concentrated acids was then added to the sample.
- Next, using a hot plate, we heated the digestion vessel containing the acid and sample at  $120\text{--}200^\circ\text{C}$  for 6 to 7 hours while constantly monitoring.
- However, the ash samples (A2, A3, A4, A5) and two FEN samples (FEN 5, 7) still contained some undigested material.
- Therefore, we transferred these sample solutions to Teflon vessels and we added 1 ml of  $\text{HF}$  to ensure proper digestion.
- Borax solution was then added to neutralize  $\text{HF}$ , and we continued heating for one more day until transparent solutions with no undigested material remained.
- Once completed, we evaporated all the samples to dryness.
- Later, Dried sample dissolved in millipore water plus  $\text{HNO}_3$  for acidification.



**Fig 2.5:** Sample digestion on hot plate

## **CHAPTER-3**



### 3. RESULT & DISCUSSION

Following the XRD examination of sample A2, we identified four minerals demonstrating 100% intensity in relation to the reference peak (I/I<sub>0</sub>). These minerals include Quartz, Zircon, Orthoclase, and Andesine. It's worth noting that Orthoclase, Zircon, and Quartz showcase distinctively sharp peaks, indicating their crystalline nature and well-organized atomic structures. In contrast, Andesine and Labradorite are classified as amorphous materials. Interestingly, within this category, Labradorite demonstrates a higher level of amorphousness compared to Andesine. This finding highlights the varied degrees of crystallinity within the sample, offering valuable insights into its composition and structural attributes as deduced through XRD analysis.

In the XRD analysis of Sample A5, we identified the presence of seven minerals: Quartz, Zircon, Andesine, Bytonite (low), Labradorite (low), Labradorite (high), and Labradorite (intermediate). Notably, Labradorite (intermediate) exhibited the sharpest peak among these minerals. Both Zircon and Quartz displayed peaks of similar intensity, albeit slightly less sharp compared to Labradorite (intermediate). Conversely, Andesine, Bytonite (low), Labradorite (high), and Labradorite (low) showed peaks of lower intensity. This variation in peak sharpness and intensity offers valuable insights into the crystalline characteristics and structural differences within Sample A5, as determined through XRD analysis.

We obtained adjusted oxide values through CIPW norms. Subsequently, based on the normative mineralogy, it is evident that quartz and hypersthene are forming minerals. Therefore, the rocks are characterized as quartz normative rhyolite, as determined by XRF analysis.

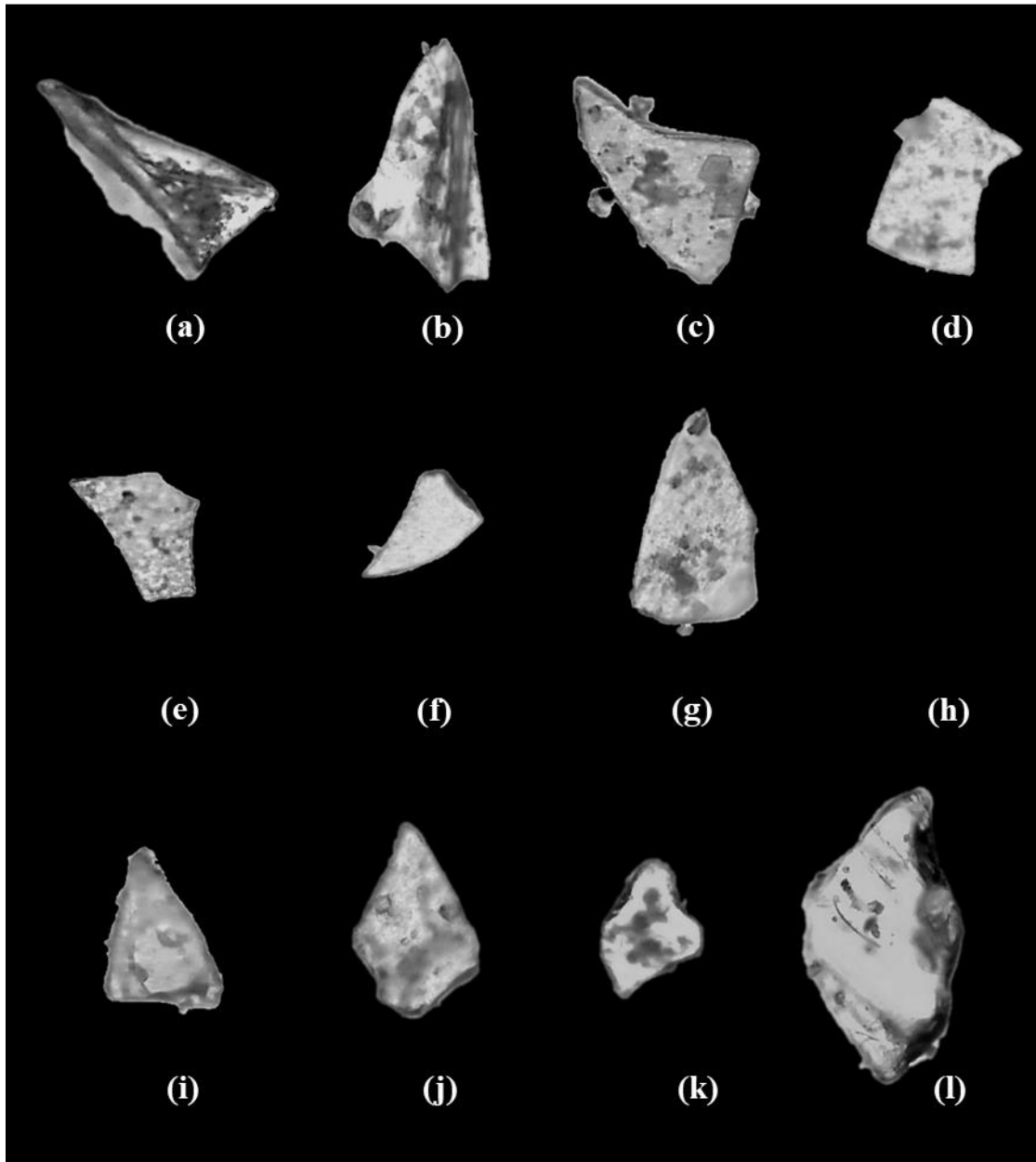


**Fig 3.1:** Photographs showing morphology of volcanic glass from ash (50 X). (a) triangular shard of glass showing ridges and depression. (b) triangular glass shard showing sharp edges. (c) triangular platy glass shard showing curved edges. (d) tabular platy glass shard with curved edges. (e) platy glass shard with sharp angular edges. (f) platy cusped glass shard with sharp edges. (g) large angular glass shards with dusty surface. (h) tabular, broken glass shard. (i) triangular stout glass shard with surface relief. (j) polygonal glass shard with ridges and pits. (k) small sub-angular piece of volcanic glass with staining. (l) Large glass shard with fluid inclusions and grooves.

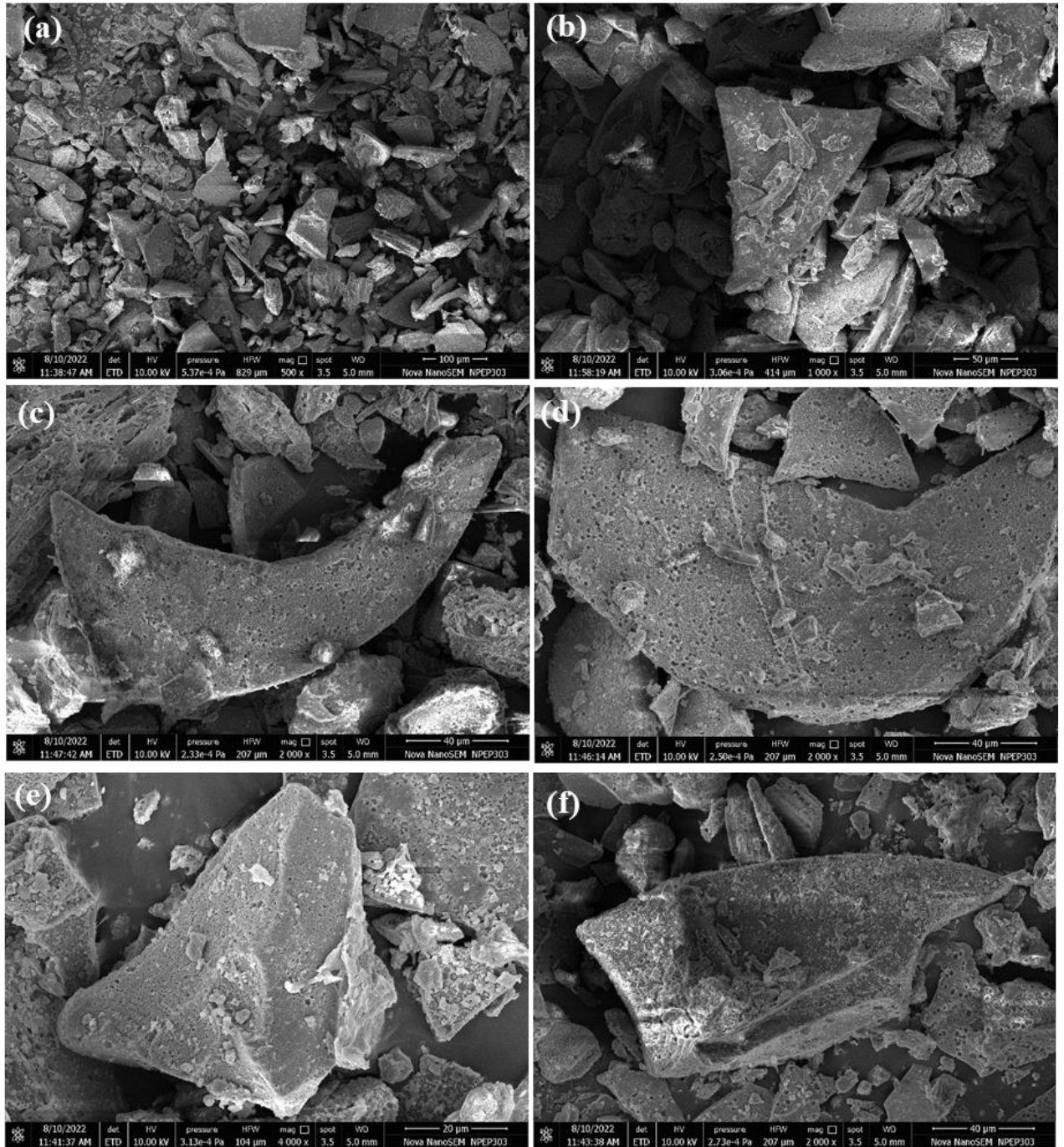


**Fig. 3.2:** Scanning Electron Microscopy (SEM) of ash from present study. (a) Aggregate of angular shards of glass constituting the ash. (b) triangular glass shard showing sharp edges. (c) another large triangular platy glass shard showing curved edges. (d) tabular platy glass shard with curved edges and showing spongy surface. (e) triangular platy glass shard with sharp angular edges. (f) platy cusped glass shard with sharp edges. (g) large angular glass shards with dusty surface. (h) tabular, broken glass shard. Note the kind of porous precipitate on the surface of all glass shards.

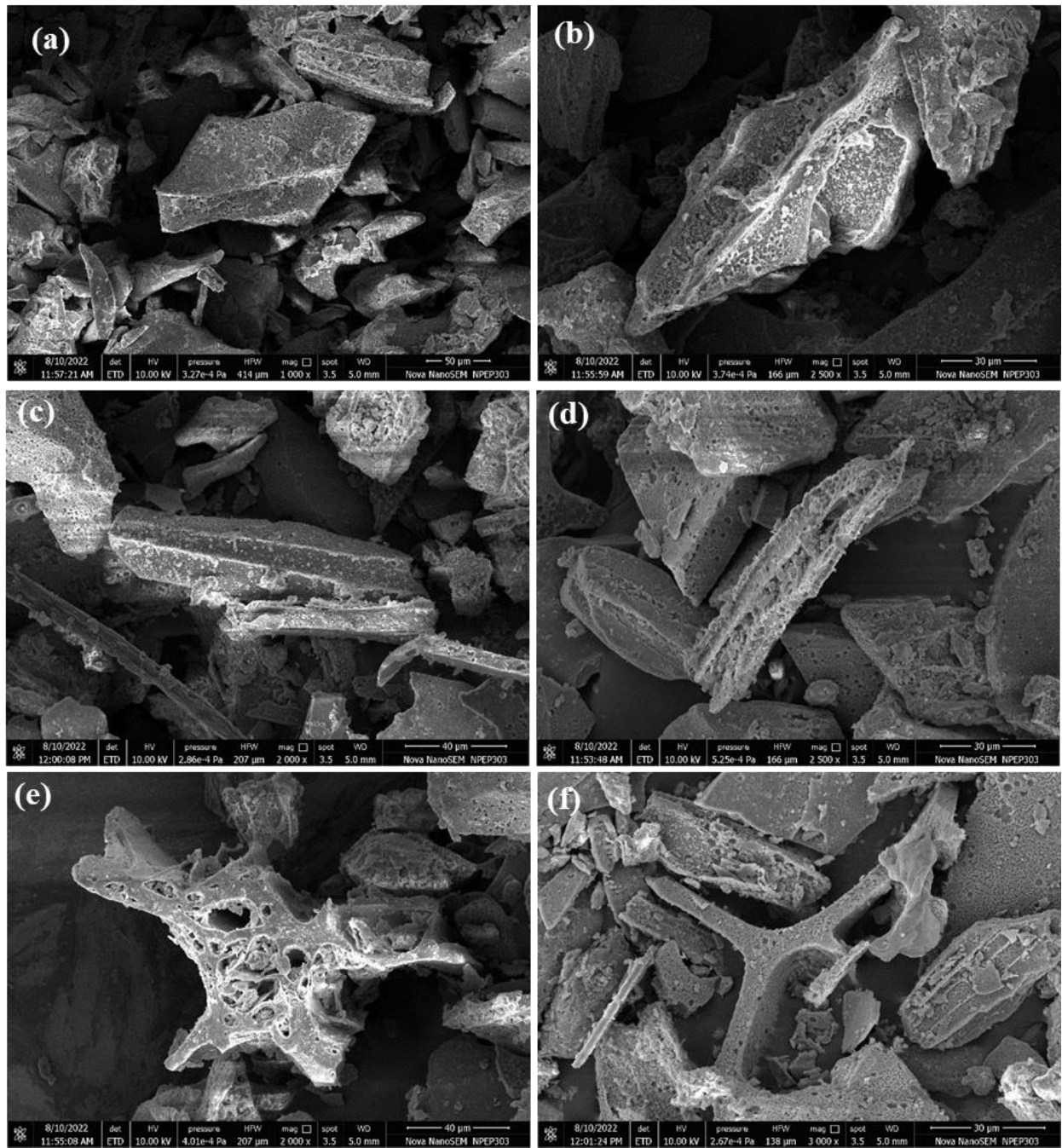


**Fig. 3.3:** Scanning Electron Microscopy (SEM) of pumecious shards from present study. (a) aggregate of stout platy shard of straw pumice showing ridges and depression. (b) another grain of stout platy shard of straw pumice. (c) Elongated fragments of pumice showing ridges and depression. (d) longitudinal section of porous pumice. (e) transverse section of winged pumice fragment with sharp edges and porous interior. (f) transverse section of a branched pumice fragment formed by the collapse of the walls of the straw pumice.



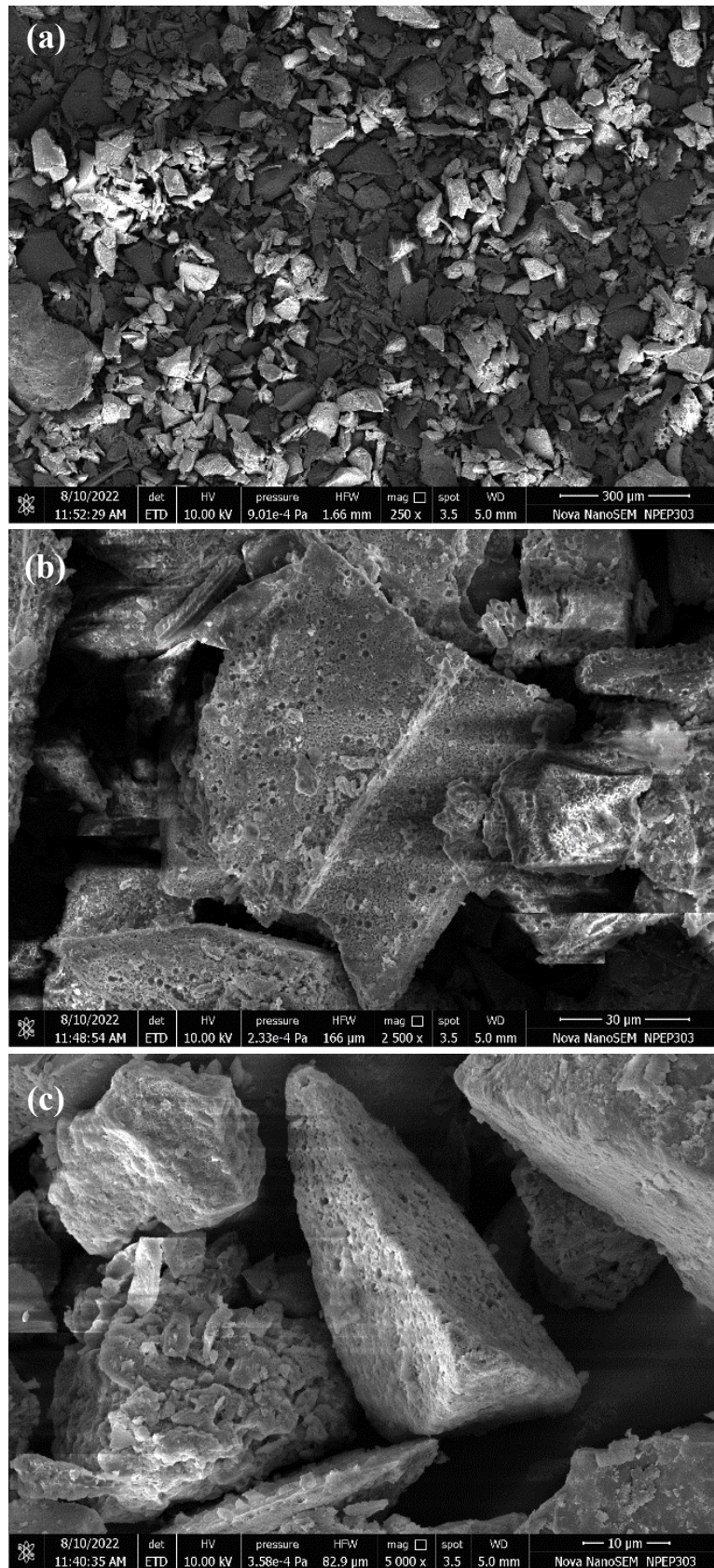


**Fig. 3.4:** Scanning Electron Microscopy (SEM) of pumecious shards from reworked horizon from the present study. (a) fine aggregate of platy shard as seen at low magnification (~300µm). (b) A stout platy shard of volcanic glass. Notice the porous surface of the shard. (c) Triangular fragments of pumice showing a uniform porous coating.

We sprinkled powdered samples on the glass slide under the petrographic microscope, and we observed triangular shards of glass showing ridges and depressions (**Fig 3.1(a)**), triangular glass shards with sharp edges (**Fig 3.1(b)**), triangular platy glass shards with curved edges (**Fig 3.1(c)**), tabular platy glass shards with curved edges (**Fig 3.1(d)**), platy glass shards with sharp angular edges (**Fig 3.1(e)**), platy cusped glass shards with sharp edges (**Fig 3.1(f)**), large angular glass shards with a dusty surface (**Fig 3.1(g)**), tabular broken glass shards (**Fig 3.1(h)**), triangular stout glass shards with surface relief (**Fig 3.1(i)**), polygonal glass shards with ridges and pits (**Fig 3.1(j)**), small sub-angular pieces of volcanic glass with staining (**Fig 3.1(k)**), large glass shards with fluid inclusions and grooves (**Fig 3.1(l)**). We also observed an aggregate of angular shards of glass constituting the ash (**Fig 3.2(a)**), triangular glass shards showing sharp edges (**Fig 3.2(b)**), another large triangular platy glass shard showing curved edges (**Fig 3.2(c)**), tabular platy glass shards with curved edges and showing a spongy surface (**Fig 3.2(d)**), triangular platy glass shards with sharp angular edges (**Fig 3.2(e)**), platy cusped glass shards with sharp edges (**Fig 3.2(f)**), large angular glass shards with a dusty surface (**Fig 3.2(g)**), tabular broken glass shards (**Fig 3.2(h)**). Note the kind of porous precipitate on the surface of all glass shards. We found pumiceous shards which show an aggregate of stout platy shards of straw pumice showing ridges and depressions (**Fig 3.3(a)**), another grain of stout platy shard of straw pumice (**Fig 3.3(b)**), elongated fragments of pumice showing ridges and depressions (**Fig 3.3(c)**), longitudinal sections of porous pumice (**Fig 3.3(d)**), transverse sections of winged pumice fragments with sharp edges and porous interiors (**Fig 3.3(e)**), transverse sections of branched pumice fragments formed by the collapse of the walls of the straw pumice (**Fig 3.3(f)**). There was also a reworked horizon (**Fig 3.4(a)**), fine aggregate of platy shards as seen at low magnification ( $\sim 300\mu\text{m}$ ), a stout platy shard of volcanic glass (**Fig 3.4(b)**), the porous surface of the shard, triangular fragments of pumice showing a uniform porous coating (**Fig 3.4(c)**).

SAMPLE	SiO <sub>2</sub>	TiO <sub>2</sub>	Al <sub>2</sub> O <sub>3</sub>	MgO	CaO	Na <sub>2</sub> O	K <sub>2</sub> O
Cryptoteph hra layer, MAL05- 1C 28.10 MBLF Average (n=18)	77.24	0.05	12.41	0.05	0.77	2.95	5.61
2 SD	1.79	0.04	0.31	0.06	0.19	0.37	0.45
Cryptoteph hra layer, MAL 05-2a 26.78 MBLF Average (n=9)	77.22	0.04	12.32	0.05	0.78	3.2	5.47
2 SD	0.47	0.05	0.27	0.03	0.21	0.26	0.26
YTT, Toba caldera Average( n=118)	77.24	0.06	12.54	0.05	0.78	3.10	5.20
2 SD	0.7	0.06	0.39	0.04	0.21	0.34	0.29
YTT, Jwalapur am, India Average (n=113)	77.36	0.36	12.49	0.07	0.75	3.25	4.93
2 SD	0.28	0.02	0.2	0.1	0.78	0.16	0.16
Maharash tra, Dahigaon Average( n=5)	73.674	0.3188	15.2014	0.6214	1.2328	3.2084	3.459
2 SD	1.75669 63	0.132215	0.761431	0.223886 6	0.2055743	0.1828912	0.1439236

**Table 3.1:** Chemical composition of YTT glass shards in Lake Malawi, compared with proximal samples from the Toba caldera in Sumatra, Indonesia, YTT ash from the Indian archaeological site of Jwalapuram and Satara, Maharashtra (Lane et al., 2013)[1]

From (**Table 3.1**) we can observe that there is slight variation in the oxide (wt.%) values due to reworked setting happened due to erosion

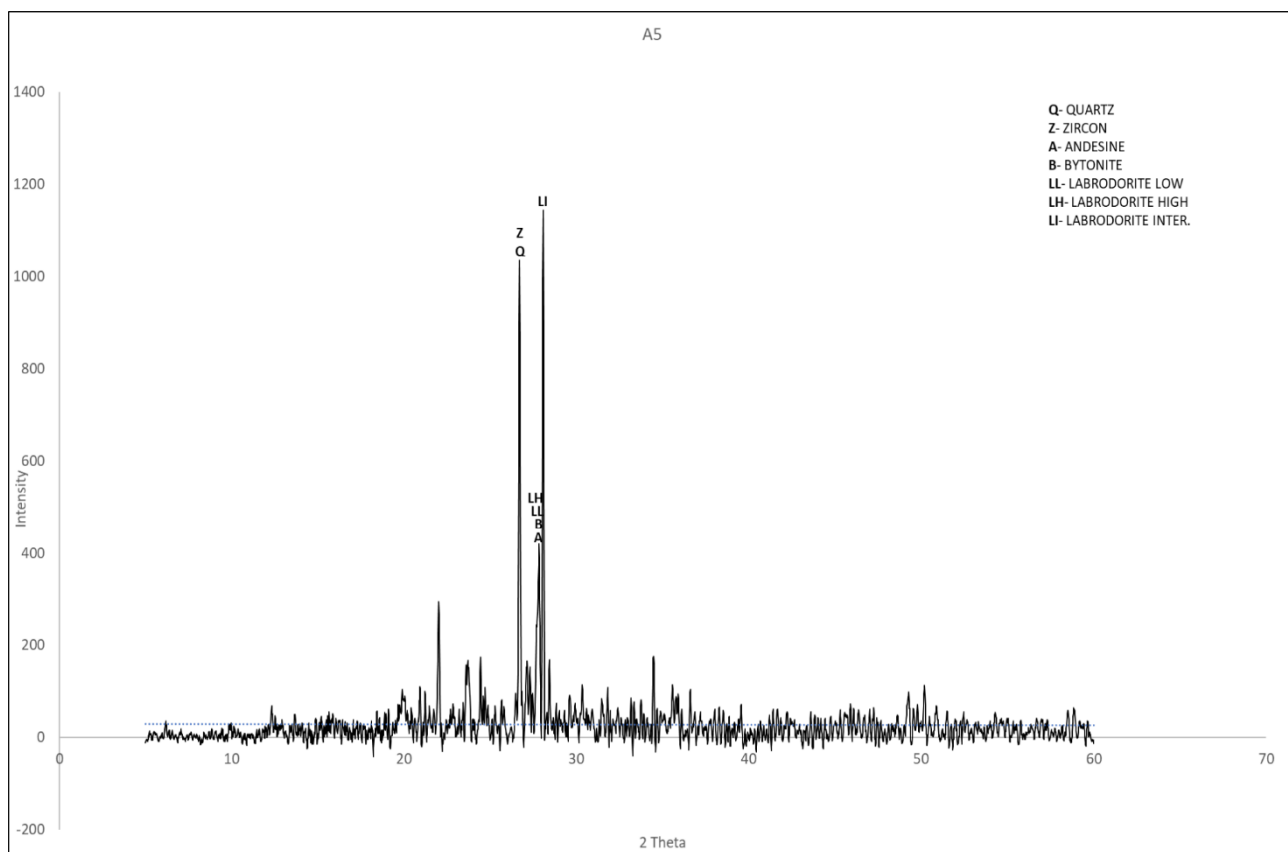
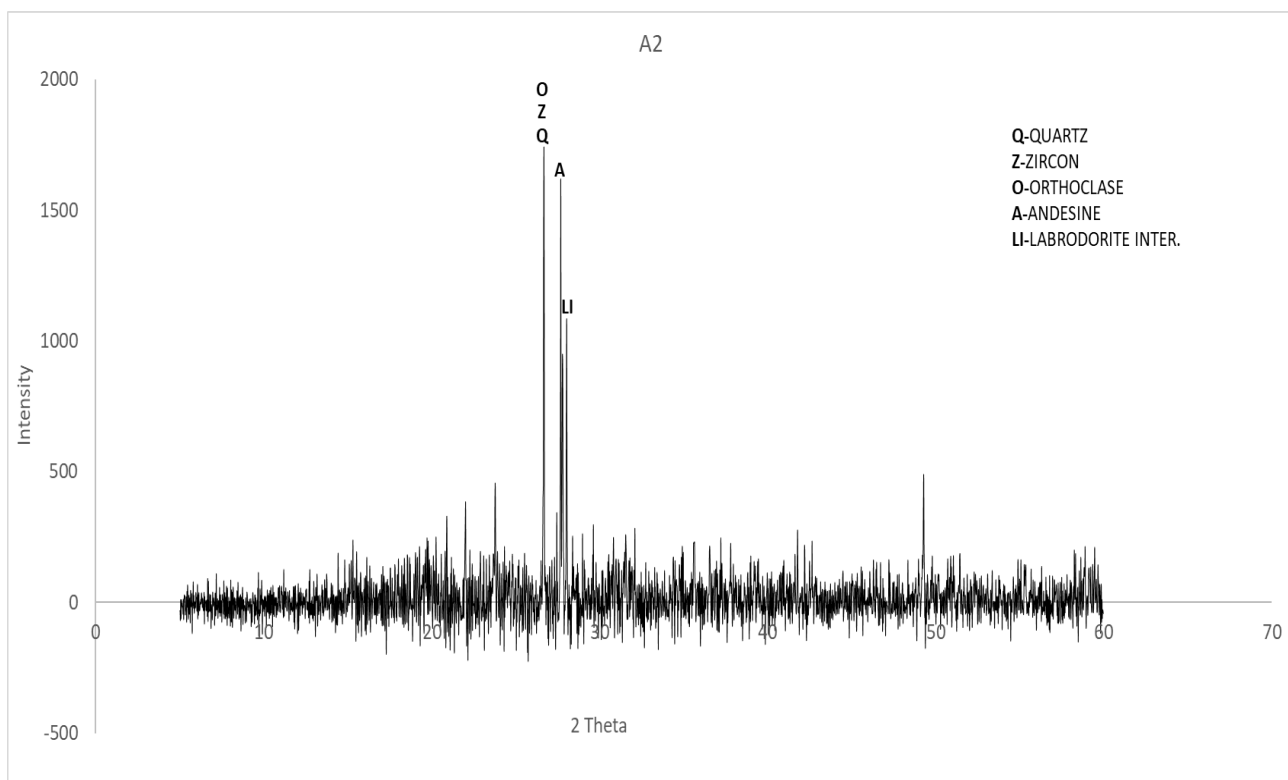


**Fig 3.5:** XRD patterns of A2 and A5 sample



<b>SAMPLE</b>	<b>MINERALS</b>	<b>DESPACING</b>	<b>I/IO</b>
<b>A2</b>	<b>QUARTZ</b>	<b>3.337</b>	<b>100</b>
		<b>4.246</b>	<b>22</b>
		<b>1.847</b>	<b>14</b>
		<b>2.414</b>	<b>8</b>
	<b>ZIRCON</b>	<b>3.337</b>	<b>100</b>
		<b>2.516</b>	<b>45</b>
	<b>ORTHOCLASE</b>	<b>3.337</b>	<b>100</b>
		<b>4.24</b>	<b>70</b>
	<b>ANDESINE</b>	<b>3.219</b>	<b>100</b>
		<b>3.179</b>	<b>90</b>
		<b>4.033</b>	<b>80</b>
		<b>2.516</b>	<b>70</b>
		<b>3.012</b>	<b>60</b>
	<b>LABRADORITE(INTE RMEDIATE)</b>	<b>3.179</b>	<b>100</b>
		<b>3.219</b>	<b>70</b>
<b>A5</b>	<b>QUARTZ</b>	<b>3.335</b>	<b>100</b>
	<b>ZIRCON</b>	<b>3.335</b>	<b>100</b>
		<b>2.601</b>	<b>45</b>
	<b>ANDESINE</b>	<b>3.203</b>	<b>100</b>
		<b>3.175</b>	<b>90</b>
		<b>4.037</b>	<b>80</b>
		<b>3.640</b>	<b>70</b>
		<b>3.134</b>	<b>70</b>
	<b>BYTONITE (LOW)</b>	<b>3.203</b>	<b>100</b>
		<b>4.037</b>	<b>80</b>
		<b>3.175</b>	<b>80</b>
	<b>LABRADORITE (LOW)</b>	<b>3.203</b>	<b>100</b>
		<b>3.175</b>	<b>90</b>
		<b>4.037</b>	<b>80</b>
		<b>3.640</b>	<b>70</b>
	<b>LABRADORITE (HIGH)</b>	<b>3.203</b>	<b>100</b>
		<b>4.037</b>	<b>80</b>
		<b>3.134</b>	<b>60</b>
	<b>LABRADORITE (INTERMEDIATE)</b>	<b>3.175</b>	<b>100</b>
		<b>3.203</b>	<b>70</b>

**Table 3.2:** A2 and A5 sample diffraction data for minerals

**Table 3.3:** Oxide percentage (wt.%) of volcanic ash samples from present study

Sample	A1	A2	A2 Rpt	A3	A4	A5
Rock type	R	R	R	R	R	R
SiO <sub>2</sub>	65.849	65.989	66.01	66.7	66.894	67.36
TiO <sub>2</sub>	0.332	0.364	0.365	0.283	0.24	0.221
Al <sub>2</sub> O <sub>3</sub>	14.364	13.752	13.807	13.708	13.439	13.408
FeOT	2.205	2.203	2.196	1.844	1.714	1.511
MnO	0.069	0.068	0.068	0.068	0.068	0.068
MgO	0.669	0.66	0.654	0.544	0.504	0.431
CaO	1.154	1.256	1.26	1.097	1.038	1.025
Na <sub>2</sub> O	2.854	2.816	2.824	2.895	2.904	3.024
K <sub>2</sub> O	3.136	3.108	3.119	3.241	3.061	3.079
P <sub>2</sub> O <sub>5</sub>	0.038	0.038	0.038	0.034	0.033	0.032
Total	90.67	97.054	97.149	96.833	96.425	96.421
SiO <sub>2</sub> adj	72.564	73.053	73.006	73.72	74.364	74.669
TiO <sub>2</sub> adj	0.366	0.403	0.404	0.313	0.267	0.245
Al <sub>2</sub> O <sub>3</sub> adj	15.829	15.224	15.27	15.151	14.94	14.863
Fe <sub>2</sub> O <sub>3</sub> adj	0.838	0.841	0.838	0.703	0.657	0.578
FeOadj	1.676	1.682	1.675	1.406	1.314	1.155
MnOadj	0.076	0.075	0.075	0.075	0.076	0.075
MgOadj	0.737	0.731	0.723	0.601	0.56	0.478
CaOadj	1.272	1.39	1.394	1.212	1.154	1.136
Na <sub>2</sub> Oadj	3.145	3.117	3.123	3.2	3.228	3.352
K <sub>2</sub> Oadj	3.456	3.441	3.45	3.582	3.403	3.413
P <sub>2</sub> O <sub>5</sub> adj	0.042	0.042	0.042	0.038	0.037	0.035
Q	36.462	36.953	36.845	37.272	38.646	38.434
Or	20.423	20.335	20.388	21.168	20.11	20.17
Ab	26.612	26.375	26.426	27.077	27.314	28.364
An	6.036	6.622	6.641	5.764	5.483	5.407
C	4.702	3.945	3.964	3.897	3.936	3.673
Hy	3.757	3.688	3.656	3.12	2.965	2.568
Mt	1.215	1.219	1.215	1.019	0.952	0.838
Il	0.695	0.765	0.767	0.594	0.507	0.465
Ap	0.097	0.097	0.097	0.088	0.086	0.081
Mg#	43.942	43.652	43.484	43.245	43.172	42.453
FeOT/MgO	3.297	3.336	3.36	3.392	3.402	3.504
Salic	89.533	90.285	90.3	91.281	91.553	92.375
Femic	5.667	5.672	5.638	4.733	4.424	3.871
Cl	7.322	7.898	7.903	6.813	6.46	6.241
DI	83.497	83.663	83.659	85.517	86.07	86.968

SI	7.481	7.45	7.371	6.332	6.112	5.325
AR	2.164	2.201	2.199	2.285	2.34	2.442

The trends evident in XRF analysis, notably observed in elemental ratios like SiO<sub>2</sub> vs Mg#, Al<sub>2</sub>O<sub>3</sub> vs Mg#, TiO<sub>2</sub> vs Mg#, FeOT vs Mg#, CaO vs Mg#, P<sub>2</sub>O<sub>5</sub> vs Mg#, P<sub>2</sub>O<sub>5</sub> vs SiO<sub>2</sub>, and TiO<sub>2</sub> vs SiO<sub>2</sub>, reveal the intricate interactions of geological processes influencing the petrogenesis of the samples. The decreasing patterns in SiO<sub>2</sub> vs Mg# and Al<sub>2</sub>O<sub>3</sub> vs Mg# suggest the impact of magmatic differentiation and fractional crystallization, where the selective crystallization of silica-rich minerals leads to SiO<sub>2</sub> enrichment while magnesium-rich minerals result in a decline in Mg#. Similarly, the increasing trends in TiO<sub>2</sub> vs Mg# and FeOT vs Mg# indicate analogous processes, with titanium-rich and iron-rich minerals affecting TiO<sub>2</sub> and FeOT concentrations, respectively, during magma evolution. The relatively constant slopes in CaO vs Mg# and P<sub>2</sub>O<sub>5</sub> vs Mg# imply limited influence from magmatic differentiation, indicating consistent crystallization behaviors for calcium-magnesium and phosphorus-magnesium minerals, likely reflecting stable magma source compositions. Moreover, the slight downward trends in P<sub>2</sub>O<sub>5</sub> vs SiO<sub>2</sub> and TiO<sub>2</sub> vs SiO<sub>2</sub> suggest the complex effects of magmatic differentiation, fractional crystallization, and magma mixing on elemental ratios across the magmatic history of the samples. These insights drawn from XRF analysis offer valuable perspectives into the geological processes steering magma development and the consistency of elemental ratios throughout, thereby enhancing our understanding of the evolutionary dynamics within the studied geological system.

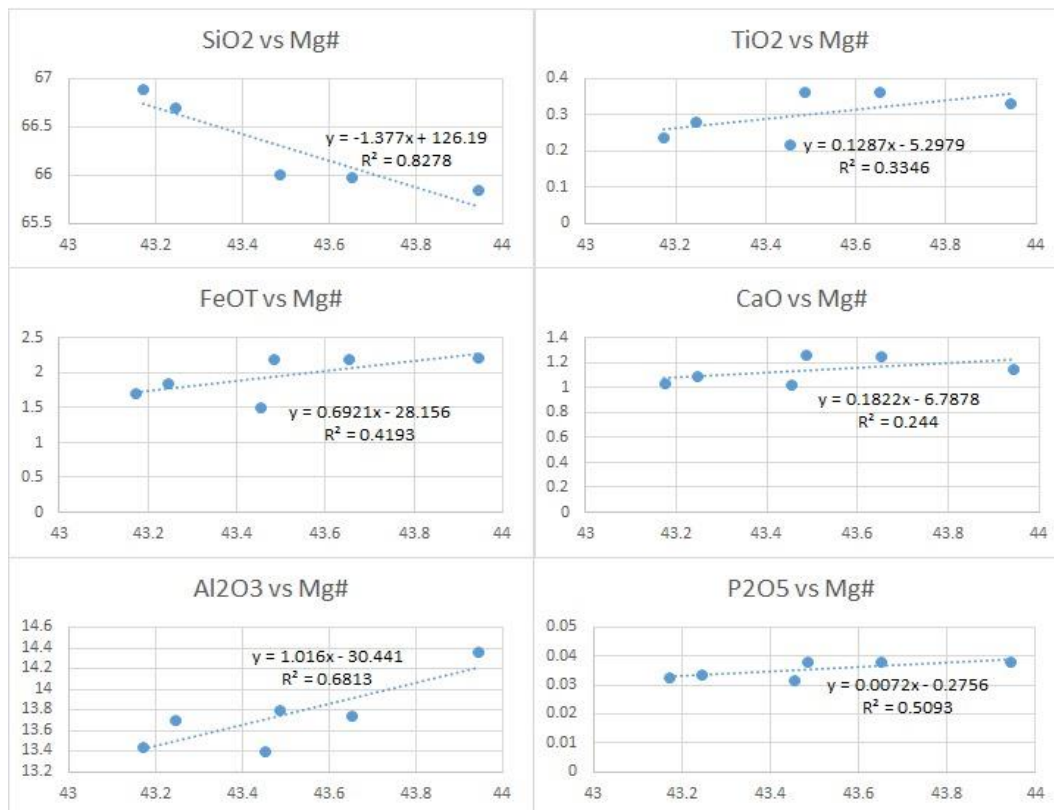


**Fig 3.6:** Graphs of Mg number vs various oxides

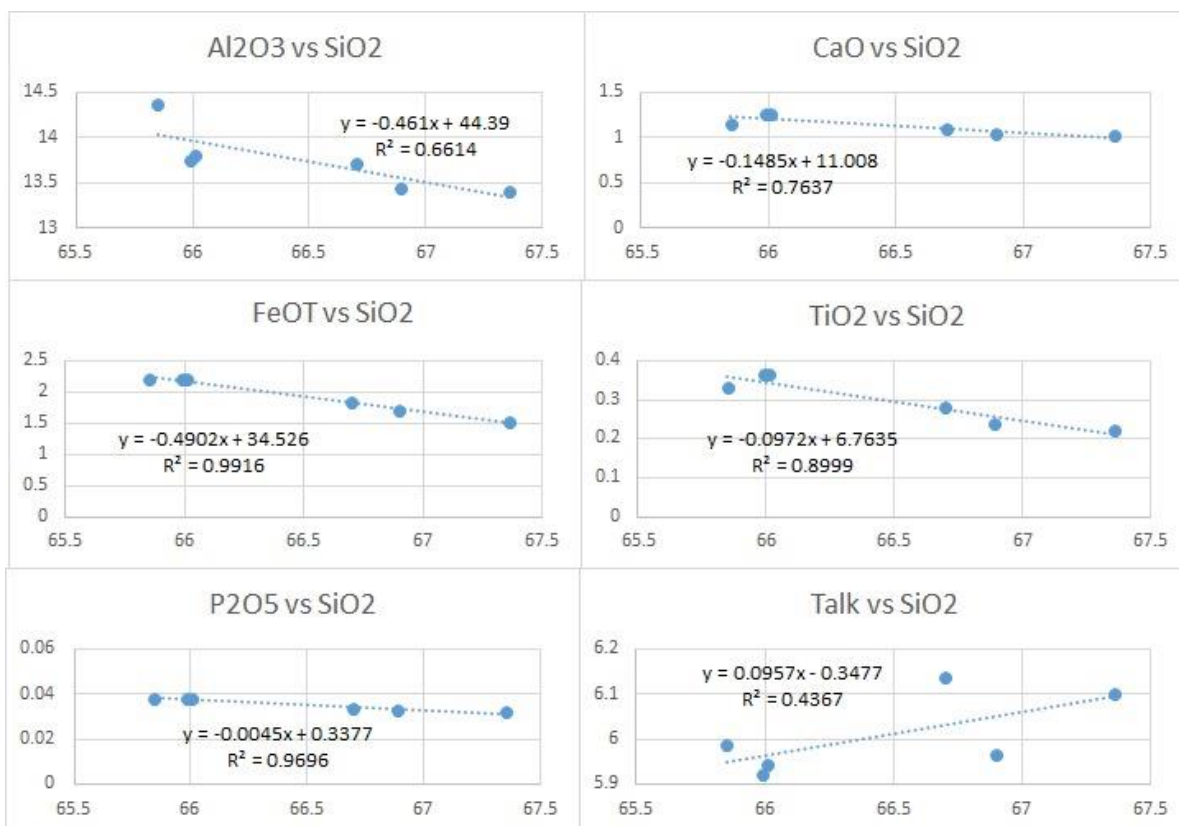


**Fig 3.7:** Graphs of SiO<sub>2</sub> versus various oxides

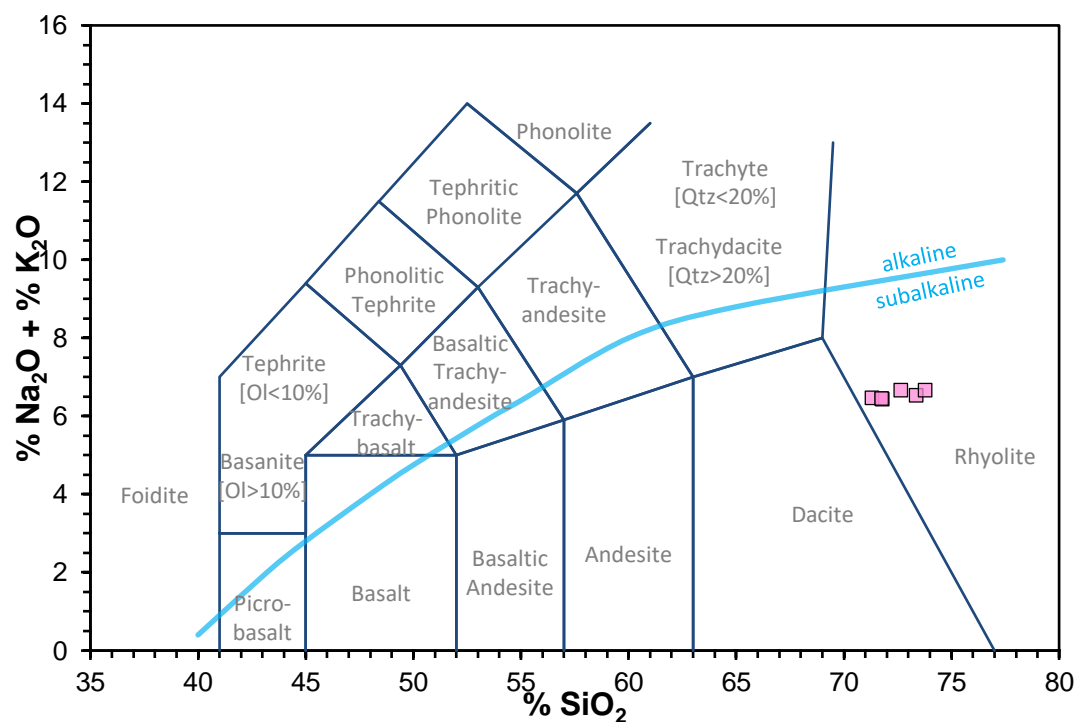


**Fig 3.8:** TAS diagram

**Table 3.3:** Oxide percentage (wt.%) of volcanic ash samples from present study

	A2	A4	Avg.
<b>7 Li</b>	8.82	7.854	8.34
<b>9 Be</b>	3.541	3.147	3.34
<b>24 Mg</b>	16780.51	9761.006	13270.76
<b>44 Ca</b>	54147.35	34086.94	44117.14
<b>45 Sc</b>	219.701	117.381	168.54
<b>47 Ti</b>	2305.094	1230.105	1767.60
<b>51 V</b>	289.591	41.355	165.47
<b>52 Cr</b>	186.486	122.777	154.63
<b>55 Mn</b>	840.37	626.925	733.65
<b>56 Fe</b>	22336.81	17693.22	20015.02
<b>59 Co</b>	14.605	10.522	12.56
<b>60 Ni</b>	70.666	92.093	81.38
<b>63 Cu</b>	151.715	128.482	140.10
<b>66 Zn</b>	338.32	182.956	260.64
<b>71 Ga</b>	30.296	24.672	27.48
<b>72 Ge</b>	2.981	2.239	2.61
<b>75 As</b>	39.395	9.24	24.32
<b>78 Se</b>	0.127	0.142	0.13
<b>85 Rb</b>	121.908	113.113	117.51
<b>88 Sr</b>	227.537	209.297	218.42

<b>89 Y</b>	76.864	74.875	75.87
<b>90 Zr</b>	725.841	563.893	644.87
<b>93 Nb</b>	21.318	23.933	22.63
<b>95 Mo</b>	3.504	4.672	4.09
<b>107 Ag</b>	0.372	0.366	0.37
<b>111 Cd</b>	1.246	0	0.62
<b>115 In</b>	0.705	0.939	0.82
<b>118 Sn</b>	23.625	40.173	31.90
<b>121 Sb</b>	0.43	0.43	0.43
<b>125 Te</b>	0.019	0	0.01
<b>133 Cs</b>	9.709	5.871	7.79
<b>137 Ba</b>	794.862	767.583	781.22
<b>139 La</b>	88.046	75.68	81.86
<b>140 Ce</b>	113.219	105.588	109.40
<b>141 Pr</b>	20.055	15.492	17.77
<b>146 Nd</b>	61.794	61.794	61.79
<b>147 Sm</b>	13.996	9.797	11.90
<b>153 Eu</b>	1.993	0.996	1.49
<b>157 Gd</b>	16.839	14.517	15.68
<b>159 Tb</b>	1.592	1.354	1.47
<b>163 Dy</b>	10.417	9.744	10.08
<b>165 Ho</b>	1.833	2	1.92
<b>166 Er</b>	12.336	10.654	11.50
<b>169 Tm</b>	1.926	1.037	1.48
<b>172 Yb</b>	17	10.737	13.87
<b>175 Lu</b>	0.649	0.649	0.65
<b>178 Hf</b>	14.214	9.239	11.73
<b>181 Ta</b>	2.074	2.345	2.21
<b>182 W</b>	0.997	3.702	2.35
<b>205 Tl</b>	0.807	0.451	0.63
<b>208 Pb</b>	14.024	13.391	13.71
<b>209 Bi</b>	0.037	0.032	0.03
<b>232 Th</b>	63.056	56.028	59.54
<b>238 U</b>	5.311	4.91	5.11

Pumice is a light, porous, and vesicular volcanic rock formed during explosive eruptions. It is sometimes referred to as a "frothy" volcanic rock because it contains many gas bubbles or vesicles, making it extremely lightweight. Glass shards are bits of volcanic glass formed when molten lava is rapidly quenched or cooled, generally as a result of the explosive character of some volcanic eruptions. The end product is a brittle, pointy, and frequently transparent to opaque substance.

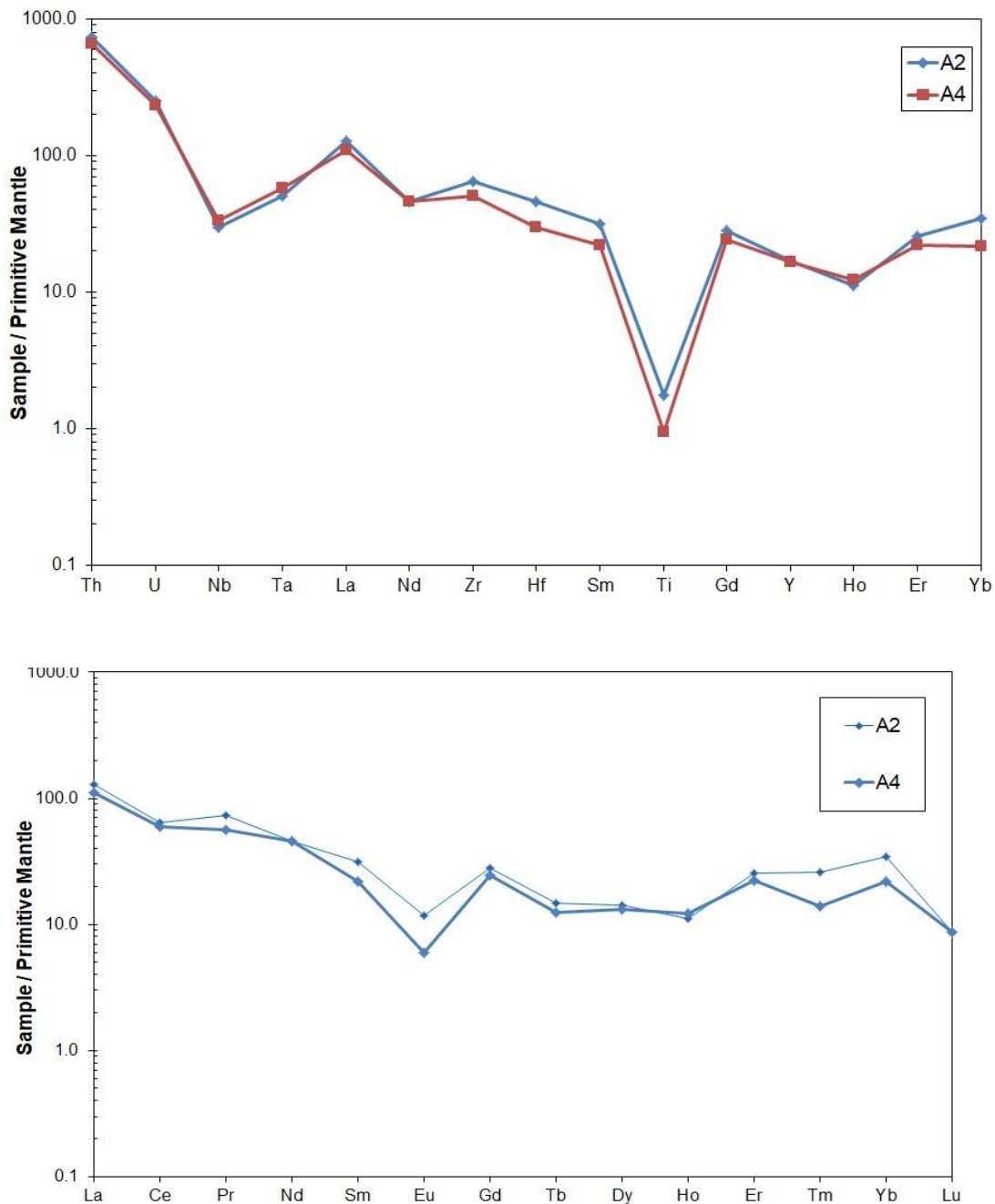


**Fig 3.9:**

The decreasing trend observed from Th to Nb, followed by an increasing trend from Nb to La, suggests a notable shift in elemental abundance patterns within this range. This declining slope from Th to Nb may imply a preferential depletion or removal of these elements relative to the primitive mantle composition, while the subsequent increasing slope from Nb to La suggests enrichment or accumulation of these elements. Additionally, the nearly constant slopes noted from Nd to Sm and from Gd to Yb imply relatively consistent partitioning

behavior for these elements compared to primitive mantle values, indicating their similar affinities or tendencies for incorporation into minerals during geological processes. Abrupt changes in slope, like the sudden decrease from Sm to Ti and subsequent increase from Ti to Gd, could potentially denote boundaries or transitions between distinct geochemical reservoirs or processes, possibly representing phase changes, mixing zones, or other geological discontinuities. The declining trend from La to Eu, followed by a rising trend from Eu to Gd, indicates changes in elemental abundance patterns within this range. This might reflect differential fractionation or enrichment mechanisms influencing certain elements during geological events. The decreasing slope from La to Eu could imply preferential depletion or removal of these elements relative to the basic mantle composition, whereas the increasing slope from Eu to Gd supports enrichment or accumulation of these elements. The almost continuous slope from Gd to Lu suggests that these elements have reasonably consistent partitioning behavior when compared to primitive mantle values. This suggests that these elements may have comparable affinities or dispositions to be absorbed into minerals throughout geological processes, resulting in consistent abundances over this range.



# **CHAPTER-4**

## CONCLUSION

The white horizon in Dahigaon exposed in the Quaternary is confirmed as a new occurrence of volcanic ash. Petrographic observation under a binocular microscope indicates that the ash is slightly altered but consists of shards and pumice fragments. The pumice fragments indicate a violent explosion at the vent. The SEM studies confirm petrographic observations. In SEM studies, we recorded the presence of curved glass shards; these glass shards are angular to sub-angular with sharp edges and show spongy precipitate on their surface. The ash deposit also contains a few fragments of straw pumice. The pumice is completely shattered, consisting of elongated, ridged, and furrowed shards that are extremely porous. The reworked ash in the brown silty mud above the ash layer also qualifies as volcanic ash. Based on field petrographic and SEM studies, we conclude that volcanic ash reworked in Quaternary deposits occurs at Dahigaon. The geochemistry of the volcanic ash suggests SiO<sub>2</sub> between 72-74 (wt.%). When plotted on the TAS diagram, the bulk chemistry of the ash confirms silicic volcanism, i.e., the composition of the ash is Rhyolitic. XRD studies of the ash show the presence of Volcanic glass and traces of quartz, plagioclase, feldspar, and minor zircon. When the Mg number versus various oxides and the SiO<sub>2</sub> versus various were plotted, the geochemical variations suggest a dominant role of fractional crystallization. Trace element geochemistry of the volcanic ash shows that the ash is typically silicic, with higher strontium ranging from (209 to 227 ppm), high zircon (563 to 725 ppm), Uranium content ranging from (4.9 to 5.3 ppm), Thorium content ranging from (56 to 63 ppm), all suggesting silicic volcanism. In the primitive mantle normalized diagram, the trace elements suggest moderate enrichment of LREE compared to HREE. The strong europium anomaly suggests plagioclase fractionation. The primitive mantle normalized diagram shows negative Nb, Nd, and Ti confirming subduction zone or island arc volcanism.

## Bibliography

- [1]. Lane, C. S., Chorn, B. T., & Johnson, T. C. (2013, April 29). Ash from the Toba supereruption in Lake Malawi shows no volcanic winter in East Africa at 75 ka. *Proceedings of the National Academy of Sciences*, 110(20), 8025–8029. <https://doi.org/10.1073/pnas.1301474110>
- [2]. Rose, W. I., & Chesner, C. A. (1990, December). Worldwide dispersal of ash and gases from earth's largest known eruption: Toba, Sumatra, 75 ka. *Palaeogeography, Palaeoclimatology, Palaeoecology*, 89(3), 269–275. [https://doi.org/10.1016/0031-0182\(90\)90068-i](https://doi.org/10.1016/0031-0182(90)90068-i)
- [3]. Alraddadi, S., & Assaedi, H. (2020, October). Characterization and potential applications of different powder volcanic ash. *Journal of King Saud University - Science*, 32(7), 2969–2975. <https://doi.org/10.1016/j.jksus.2020.07.019>
- [4]. Matthews, N. E., Smith, V. C., Costa, A., Durant, A. J., Pyle, D. M., & Pearce, N. J. (2012, May). Ultra-distal tephra deposits from super-eruptions: Examples from Toba, Indonesia and Taupo Volcanic Zone, New Zealand. *Quaternary International*, 258, 54–79. <https://doi.org/10.1016/j.quaint.2011.07.010>
- [5]. Song, S. R., Chen, C. H., Lee, M. Y., Yang, T., Iizuka, Y., & Wei, K. Y. (2000, July). Newly discovered eastern dispersal of the youngest Toba Tuff. *Marine Geology*, 167(3–4), 303–312. [https://doi.org/10.1016/S0025-3227\(00\)00034-7](https://doi.org/10.1016/S0025-3227(00)00034-7)
- [6]. Rose, W. I., & Chesner, C. A. (1987). Dispersal of ash in the great Toba eruption, 75 ka. *Geology*, 15(10), 913. [http://dx.doi.org/10.1130/0091-7613\(1987\)15<913:doaitg>2.0.co;2](http://dx.doi.org/10.1130/0091-7613(1987)15<913:doaitg>2.0.co;2)
- [7]. Floor, G. H., Marguá, E., Hidalgo, M., Queralt, I., Kregsamer, P., Streli, C., & Román-Ross, G. (2013, August). Study of selenium sorption processes in volcanic ash using Total Reflection X-ray Fluorescence (TXRF). *Chemical Geology*, 352, 19–26. <https://doi.org/10.1016/j.chemgeo.2013.05.034>
- [8]. Williams, M. (2012, May). The ~73 ka Toba super-eruption and its impact: History of a debate. *Quaternary International*, 258, 19–29. <https://doi.org/10.1016/j.quaint.2011.08.025>
- [9]. Verma, S. P., Torres-Alvarado, I. S., & Sotelo-Rodríguez, Z. T. (2002, June). SINCLAS: standard igneous norm and volcanic rock classification system. *Computers & Geosciences*, 28(5), 711–715. [https://doi.org/10.1016/S0098-3004\(01\)00087-5](https://doi.org/10.1016/S0098-3004(01)00087-5)
- [10]. Chesner, C. A. (1998, March 1). Petrogenesis of the Toba Tuffs, Sumatra, Indonesia. *Journal of Petrology*, 39(3), 397–438. <https://doi.org/10.1093/petroj/39.3.397>
- [11]. Chesner, C.A., Rose, W.I. Stratigraphy of the Toba Tuffs and the evolution of the Toba Caldera Complex, Sumatra, Indonesia. *Bull Volcanol* **53**, 343–356 (1991). <https://doi.org/10.1007/BF00280226>
- [12]. Liu, P., Chung, S., Chesner, C. A., Gao, M., Lai, Y., Lee, H., & Yang, Y. (2022, December). New Insights Into the Petrogenesis of Voluminous Crustal-Signature Silicic

Volcanic Rocks of the Toba Eruptions (Indonesia). *Journal of Geophysical Research: Solid Earth*, 127(12). <https://doi.org/10.1029/2022jb024559>

[13]. Alraddadi, S. (2020). Surface and thermal properties of fine black and white volcanic ash. *Materials Today: Proceedings*, 26, 1964–1966. <https://doi.org/10.1016/j.matpr.2020.02.429>

[14]. Bunga Naen, G. N. R., Toramaru, A., Miyamoto, T., & Wibowo, H. E. (2020, March 23). *The Youngest Toba Tuff (74 ka) Crystals Characterization*. <https://doi.org/10.5194/egusphere-egu2020-6694>

[15]. Gasparotto, G., Spadafora, E., Summa, V., & Tateo, F. (2000, January). Contribution of grain size and compositional data from the Bengal Fan sediment to the understanding of Toba volcanic event. *Marine Geology*, 162(2–4), 561–572. [https://doi.org/10.1016/s0025-3227\(99\)00090-0](https://doi.org/10.1016/s0025-3227(99)00090-0)

[16]. Chesner, C. A., Barbee, O. A., & McIntosh, W. C. (2020, February 13). The enigmatic origin and emplacement of the Samosir Island lava domes, Toba Caldera, Sumatra, Indonesia. *Bulletin of Volcanology*, 82(3). <https://doi.org/10.1007/s00445-020-1359-9>

[17]. Gatti, E. (2013). Geochemical and sedimentological investigations of Youngest Toba Tuff ashfall deposits. <https://doi.org/10.17863/CAM.16436>

[18]. Kutterolf, S., Schindlbeck-Belo, J., Müller, F., Pank, K., Lee, H. Y., Wang, K. L., & Schmitt, A. (2023, September). Revisiting the occurrence and distribution of Indian Ocean Tephra: Quaternary marine Toba ash inventory. *Journal of Volcanology and Geothermal Research*, 441, 107879. <https://doi.org/10.1016/j.jvolgeores.2023.107879>

[19]. Srivastava, A. K., Singh, A., Muhammad, R. F. B. H., Pattan, J., Sharma, N., Parthiban, G., & Khare, N. (2021, September 15). Geochemical characterization and regional correlation of Youngest Toba Tuff (YTT, 75 ka) glass shards, Purna alluvial basin, Central India. *Arabian Journal of Geosciences*, 14(19). <https://doi.org/10.1007/s12517-021-07848-z>

[20]. PEARCE, N. J. G., WESTGATE, J. A., GATTI, E., PATTAN, J. N., PARTHIBAN, G., & ACHYUTHAN, H. (2014, October 21). Individual glass shard trace element analyses confirm that all known Toba tephra reported from India is from the c. 75-ka Youngest Toba eruption. *Journal of Quaternary Science*, 29(8), 729–734. <https://doi.org/10.1002/jqs.2741>